

# Neural activity sequences arising from spatially correlated asymmetry in EI-networks

A Thesis

submitted to

Indian Institute of Science Education and Research Pune  
in partial fulfillment of the requirements for the  
BS-MS Dual Degree Programme

by

Shreya Lakhera



Indian Institute of Science Education and Research Pune  
Dr. Homi Bhabha Road,  
Pashan, Pune 411008, INDIA.

April, 2020

Supervisors: Prof. Upinder S. Bhalla, Dr. Arvind Kumar

© Shreya Lakhera 2020

All rights reserved

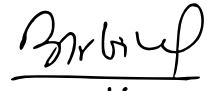


# Certificate

This is to certify that this dissertation entitled Neural activity sequences arising from spatially correlated asymmetry in EI-networks towards the partial fulfilment of the BS-MS dual degree programme at the Indian Institute of Science Education and Research, Pune represents work carried out by Shreya Lakhera at National Center for Biological Sciences, Bangalore under the supervision of Prof. Upinder S. Bhalla and at KTH Royal Institute of Technology, Stockholm under the supervision of Dr. Arvind Kumar, during the academic year 2019-2020.



Prof. Upinder S. Bhalla



Dr. Arvind Kumar



Shreya Lakhera

Committee:

Prof. Upinder S. Bhalla

Dr. Arvind Kumar

Dr. Collins Assisi



This thesis is dedicated to my mother, Kamlesh




# Declaration

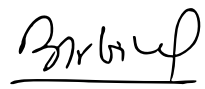
I hereby declare that the matter embodied in the report entitled Neural activity sequences arising from spatially correlated asymmetry in EI-networks are the results of the work carried out by me at the National Center for Biological Sciences, Bangalore under the supervision of Prof. Upinder S. Bhalla and at KTH Royal Institute of Technology, Stockholm under the supervision of Dr. Arvind Kumar and the same has not been submitted elsewhere for any other degree.



Shreya Lakhera



Prof. Upinder S. Bhalla



Dr. Arvind Kumar





# Acknowledgments

I wish to express my deepest gratitude to my supervisors, Upi and Arvind. Upi motivated me to do better at every step and Arvind inspired me to think in new directions. I am thankful to my labmates and friends from NCBS Bangalore for the long coffee breaks and amazing conversations. I would like to thank KVPY and DST Indo-Swedish grant for funding this project. I would also like to thank the various IT facilities at NCBS Bangalore and KTH Royal Institute of Technology, Stockholm, who were crucial in the smooth progress of the project. Lastly, I would like to thank my family and friends from IISER Pune for their unwavering support.



# Abstract

Sequential neuronal activity is associated with tasks like spatial navigation and encoding memory and time. Recently, it has been shown that correlated spatial asymmetry in recurrent excitatory connections of neurons can generate neuronal activity sequences. In present work, we show that correlated spatial asymmetry in any type of connections (i.e. excitatory (E) to inhibitory (I), I to E, and I to I) is sufficient to generate neuronal activity sequences. We found that when correlated spatial asymmetry is present in inhibitory connections, sequences are slower. In these networks, the ratio of symmetric and asymmetric connections is an important variable that determines whether the network will exhibit sequences or not and determines the stability of the ongoing activity state. On a structural level correlated asymmetric connectivity introduces effective feedforward pathways in the network, and here we demonstrate that such feedforward paths predict and are the causal mechanism behind the emergence of activity sequences. We ask if this network can show a spatially random background activity state, parallel to a biological network.



# Contents

<b>Abstract</b>	<b>xi</b>
<b>1 Introduction</b>	<b>1</b>
<b>2 Methods</b>	<b>5</b>
2.1 Neuron model . . . . .	5
2.2 Synapse model . . . . .	5
2.3 Network connectivity . . . . .	6
2.4 Input to the network . . . . .	11
2.5 Characterizing sequences . . . . .	12
2.6 Feedforward paths . . . . .	13
2.7 Search for background activity state . . . . .	17
<b>3 Results</b>	<b>21</b>
3.1 Sequential activity in networks with correlated spatial asymmetry in EI and IE connections . . . . .	21
3.2 Second model of asymmetry which includes symmetric connections also generates sequences . . . . .	22
3.3 State transition to stationary activity due to relative strength of asymmetry .	24
3.4 Embedded feedforward paths predict sequences . . . . .	26

3.5	Silencing embedded feedforward paths reduces the sequences . . . . .	28
3.6	Spatially random background activity state . . . . .	29
<b>4</b>	<b>Discussion</b>	<b>33</b>
4.1	Mechanism for sequences when spatially correlated asymmetry is present in EI, IE and II connections. . . . .	34
4.2	Feedforward paths based on connectivity can be used to predict sequences	35
4.3	Different states in new model of asymmetry . . . . .	35
4.4	Importance of spatial localization for sequential activity . . . . .	36
4.5	Spatial structure of the network and background activity state . . . . .	37
	<b>References</b>	<b>39</b>

# List of Figures

2.1	Network structure. . . . .	7
2.2	Spatial positions of postsynaptic neurons from one neuron . . . . .	8
2.3	Two models of asymmetric connections. . . . .	10
2.4	Spatial correlation in asymmetric connections . . . . .	11
2.5	Spiketime clusters for finding speed of sequences . . . . .	13
2.6	Schematic for calculation of feedforward paths . . . . .	16
3.1	Sequential activity using Model 1 of asymmetry . . . . .	22
3.2	Number and speed of sequences using Model 1 of asymmetry . . . . .	23
3.3	Sequential activity using Model 2 of asymmetry . . . . .	24
3.4	Different shapes of localized activity using Model 2 of asymmetry . . . . .	24
3.5	Number and speed of sequences using Model 2 of asymmetry . . . . .	25
3.6	Examples of stationary and sequential activity . . . . .	26
3.7	Phase plot of the network's dynamical state . . . . .	27
3.8	Examples of predicted feedforward paths and corresponding simulated activity path . . . . .	28
3.9	Similarity of predicted feedforward paths to corresponding simulated activity path . . . . .	29
3.10	Example of simulation after reduced weights of feedforward path synapses	30

3.11	Number of sequences after reducing weights of feedforward path synapses	31
3.12	Search for background activity state: Variation of network sequences on serially changing parameters . . . . .	32



# List of Tables

2.1	Leaky Integrate and Fire neuron parameters . . . . .	6
2.2	Alpha synapse parameters . . . . .	6
2.3	Common connectivity parameters for simulations . . . . .	8
2.4	Probability of connections in asymmetry model 2 . . . . .	9
2.5	Synaptic weights in model 2 of asymmetry. . . . .	10
2.6	Synaptic weights distribution in partially random networks . . . . .	18
2.7	Initial synaptic weight parameters in partially random networks . . . . .	18
2.8	List and range of values for serial parameter search for background activity state . . . . .	19



# Chapter 1

## Introduction

One of the major goals of contemporary neuroscience is to understand how the brain processes information about the external environment. This processing happens through the activity of ensembles of neurons that corresponds to a function or behavioural state. For example, the population activity of the neurons in the olfactory system represents which odor is being sensed by the animal [Krofczik et al., 2009, Mazor and Laurent, 2005]. Therefore, activity patterns in networks of neurons are important for understanding functioning of the brain.

One such network activity pattern that has been observed in multiple regions of the brain is sequential activity. Sequential neural activity refers to an ordered pattern of neurons firing in a network. In this activity pattern, the temporal sequence of neurons (firing in response to a task-related input) stays constant across trials, meaning that the order of firing is determined by some property intrinsic to the network or by a property of the sensory input. Sequential activity induced by sequential sensory input has been found in the visual cortex [Muto et al., 2013] and in the context of prediction in the auditory cortex [Bouchard and Brainard, 2016]. It has also been observed in pre-motor planning for song vocalizations [Hahnloser et al., 2002]. Sequential activity has been seen in the hippocampus while performing tasks like spatial navigation [Dragoi and Buzsáki, 2006, Dragoi and Tonegawa, 2011] and tracking time [Modi et al., 2014]. It has been seen in the striatum

and prefrontal cortex for encoding time [Bakhurin et al., 2017] and in the parietal cortex while making choices [Harvey et al., 2012]. Thus, intrinsically generated sequential activity is observed in many behaviourally relevant functions. It is intuitive that there should be sequential activity underlying behavior; any animal behavior is a well-ordered sequence of actions [Lashley, 1951] and therefore neurons encoding those behaviors must also fire in a well-ordered sequence [Hebb, 1949].

The mechanism of sequential activity generation in a network has received significant attention by computational neuroscientists in the past and several mechanisms have been proposed that can endow a network to generate sequential activity. A simple mechanism of sequence generation is a feedforward network operating in the so-called synfire mode [Abeles, 1991, Diesmann et al., 1999]. In this mechanism, ensembles of neurons preferentially project to the next group of neurons thus creating an order for the firing neurons. Such feedforward networks can be embedded in a recurrent random network and the latter can generate sequences spontaneously or in response to an external input [Kumar et al., 2008]. A big limitation of this mechanism is that the sequences have to be manually wired to generate sequential responses. Another method of creating sequential activity uses attractor networks dynamics. Here, switching between different attractors through spike threshold adaptation generates sequential activity [Azizi et al., 2013, Itskov et al., 2011]. Recurrent networks can be trained to show sequential activity dynamics using supervised learning rules [Goudar and Buonomano, 2015, Rajan et al., 2016, Sussillo and Abbott, 2009] or in some cases unsupervised learning rule [Haga and Fukai, 2018]. In some models, synaptic depression can be used to create sequential activity in recurrent networks [Murray and Escola, 2017, York and van Rossum, 2009]. A more complete overview of sequences and computational models used to explain their generation can be found in [Bhalla, 2019].

A recent study showed that if the synaptic connectivity in a neural network is asymmetrical and spatially correlated, then the network shows spontaneous spatiotemporal activity sequences [Spreizer et al., 2019]. Previous models used either biologically unfeasible connectivity or supervised learning algorithms to induce sequential activity in a network. This model provided a biologically plausible generative rule which renders the

network with an ability to exhibit sequences without explicitly learning or manual wiring of connections.

In this model, sequences were shown when asymmetry was present in recurrent connections among excitatory neurons (or among inhibitory neurons in a purely inhibitory network). In a recurrent network of excitatory and inhibitory neurons there are four different types of connections: from excitatory to excitatory neurons, from excitatory to inhibitory neurons, from inhibitory to excitatory neurons, from inhibitory to inhibitory neurons. In this work, we extend the model presented by Spreizer et al and ask if the asymmetry in any of the remaining three types of connections can also give rise to sequences. Moreover, we systematically characterize the effect of connection asymmetry on both sequential activity and the stability of the ongoing activity.

To this end we implemented a new algorithm to wire the network with correlated asymmetric connectivity in which we can not only choose the type of connections which are to be wired in an asymmetric fashion but also control the ratio of symmetric to asymmetric connections of a neuron. We observed that a network with both symmetric and asymmetric connectivity can have different dynamical states. We probed the parameter space of the model to check what can lead to the loss of activity sequences and cause different dynamical states.

We also identified the mechanism underlying the emergence of sequences in this model and asked if there exists a map from the underlying connectivity to the neural activity path. Previously Spreizer et al. showed that underlying feedforward paths in the network correlate with the presence of sequences. In this work, we verified if the feedforward paths predict and cause sequential activity in the simulated network.

A useful model needs to be relatable to the biological system it is modeling. Therefore, we ask how verifiable this model is and if it can make certain predictions for the biological system. The underlying assumption of spatially correlated asymmetry has some support from previous work [Bernard and Wheal, 1994, Ishizuka et al., 1990, Shein-Idelson et al., 2017]. However, it can be complicated to draw parallels between physical connectivity

patterns and our connectivity assumption. Instead, we suggest that neural recordings of the background activity in a network could have a signature of the structure of the network. This can be related to either the connectivity in our model or the feedforward paths and can lead to a testable prediction of the sequential paths formed in the network. For this purpose, we need our model to show a background activity state. Therefore, we asked if different kinds of input can make our model show separate background and sequential activity states.

# Chapter 2

## Methods

### 2.1 Neuron model

The neurons were modelled as leaky integrate and fire (LIF) neurons. Dynamics of each neuron was described by:

$$C_m \frac{dV_i}{dt} = -g_L(V_i - E_L) + I_{synaptic}(t) + \mu_{input} + \sigma_{input} \quad (2.1)$$

Where,  $C_m$  is membrane capacitance,  $V_i$  is the membrane potential,  $E_L$  is the leak reversal potential,  $g_L$  is the leak conductance and  $I_{synaptic}$  is the current-based synaptic input from presynaptic neurons.  $\mu_{input}$  and  $\sigma_{input}$  are the mean and standard deviation of the Gaussian white noise provided as external input to each neuron. The values of the parameters are provided in Table 2.1.

### 2.2 Synapse model

Neurons were connected using current-based synapses. Each presynaptic spike introduced an alpha function shaped voltage transient post-synaptic potential in the postsy-

Parameter	Value
Membrane capacitance $C_m$	250 pF
Leak reversal potential $E_{Leak}$	-70 mV
$t_{ref}$	2 ms
$\tau_m = C_m/g_L$	10 ms
$\tau_{minus}$	20 ms
$V_{reset}$	-70 mV
$V_{threshold}$	-55 mV

Table 2.1: Leaky Integrate and Fire neuron parameters

naptic neuron. The shape of the PSP is described as:

$$I_{synaptic}(t) = J_{syn} \frac{t - t_0}{\tau_{syn}} e^{-\frac{t-t_0}{\tau_{syn}}} \quad (2.2)$$

Where,  $t_0$  = time of spike,  $\tau_{syn}$  is the synaptic time constant and  $J_{syn}$  is the amplitude of the voltage response in the postsynaptic neurons. The value of all the parameters of excitatory and inhibitory synapses is provided in 2.2.

Parameter	Value
$\tau_{syn}$ for excitatory synapse	5 ms
$\tau_{syn}$ for inhibitory synapse	5 ms
Synaptic weight $J_{syn}$ for excitatory synapses	10
Synaptic weight $J_{syn}$ for inhibitory synapses	-80

Table 2.2: Alpha synapse parameters

## 2.3 Network connectivity

We simulated networks of 18,000 neurons (80 % excitatory and 20 % inhibitory).



### 2.3.1 Spatial arrangement of the neurons

The neurons were arranged on a square grid with periodic boundary conditions. The excitatory neuron grid was 2 times larger (4 times more number of neurons). The excitatory (E) layer was of the size 120 x 120 neurons and the inhibitory (I) layer was of size 60 x 60 neurons (Figure 2.1).

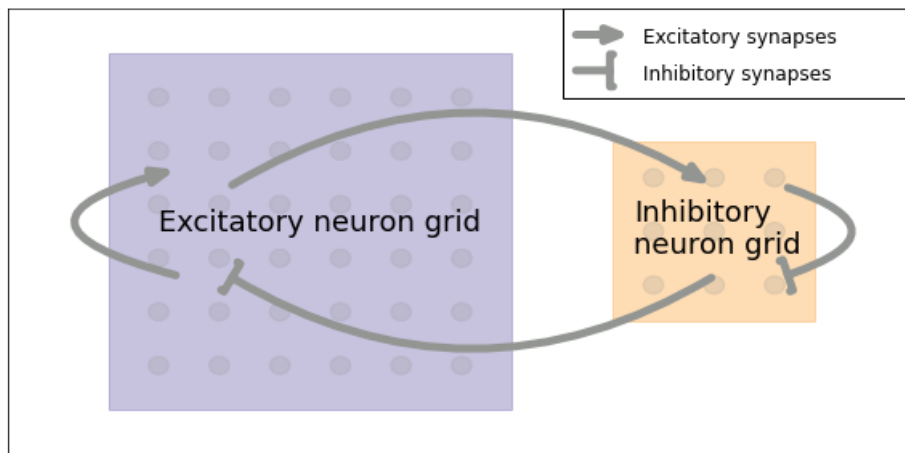


Figure 2.1: Network structure.

### 2.3.2 Spatial connectivity rule

Each neuron was modeled to have local synapses in a region around the pre-synaptic neuron (Figure 2.2). The probability of connections decreased monotonically according to a two-dimensional Gaussian function. The spatial extent of the connectivity of a neuron was determined by the standard deviation of the 2-D Gaussian function (denoted as spatial spread in Table 2.3). The probability of connection determines how many synapses a neuron sends out in this given region.

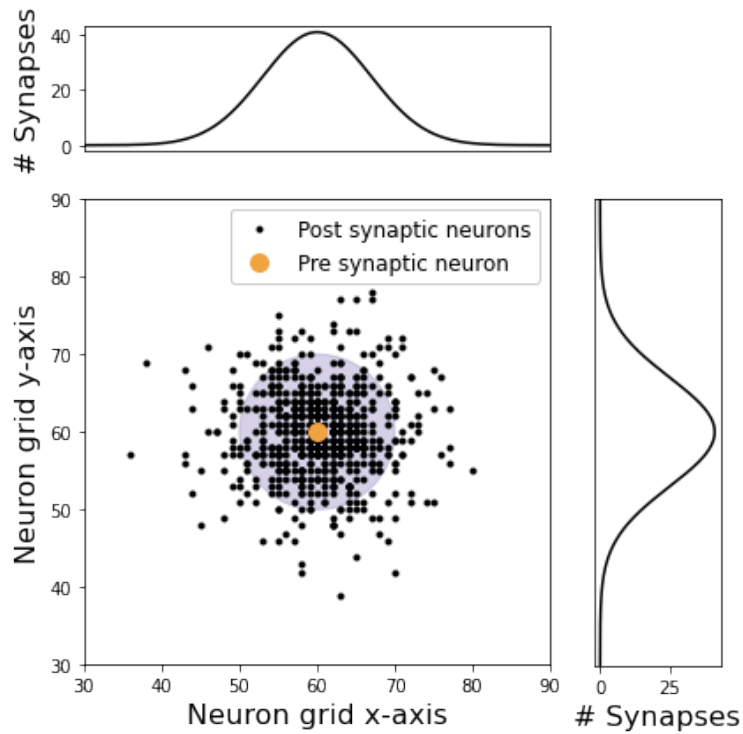


Figure 2.2: Spatial positions of local projections sent out by each neuron in the symmetric case. Purple circle denotes the region of higher projections. Curves denote the variation of number of synapses in the two axes.

Parameter	Value
Probability of (E or I) to (E or I) connections	0.05
Spatial spread of (E or I) to E connections (model 1)	4 grid points
Spatial spread of (E or I) to I connections (model 1)	6 grid points
Spatial spread of (E or I) to E connections (model 2)	7 grid points
Spatial spread of (E or I) to I connections (model 2)	9 grid points

Table 2.3: Common connectivity parameters for simulations

### 2.3.3 Spatially asymmetric connectivity: Model 1

To modify the circularly symmetric local connectivity of a region we followed the same method as used by [Spreizer et al., 2019]. In this model we shifted the entire circular projection region of a neuron in a particular direction (Figure 2.3a). The shifting of this region can be described by a vector connecting the center of the original and shifted circles. The angle of these vectors is varied from 0 to  $2\pi$ , in steps of  $\pi/4$ . Therefore, we have 8 directions of asymmetry specified by values from 0 to 7. The length of this vector determines how far the circle shifts in these directions and was set to 1 in our simulations.

### 2.3.4 Spatially asymmetric connectivity: Model 2

In the second model to introduce spatially asymmetric connectivity we wired a neuron such that it had a larger number of connections in one specific direction as compared to other directions. For each asymmetry direction  $\theta$ , we chose a sector going from  $\theta - \pi/4$  to  $\theta + \pi/4$  (Figure 2.3b). We controlled the area of this sector by specifying its outer radius (12 grid points) and inner radius (2 grid points). The relative number of synapses in the asymmetric sector vs the symmetric circle was controlled by the parameter  $\alpha$ . Any value of  $\alpha$  above 0.125 had denser directional synapses than symmetric synapses.

$$\alpha = \frac{\text{Number of synapses in sector}}{\text{Number of synapses in rest of the circle}} \quad (2.3)$$

	EE	EI	IE	II
Symmetric	$(1 - \alpha_{EE})p_{EE}$	$(1 - \alpha_{EI})p_{EI}$	$(1 - \alpha_{IE})p_{IE}$	$(1 - \alpha_{II})p_{II}$
Asymmetric	$\alpha_{EE}p_{EE}$	$\alpha_{EI}p_{EI}$	$\alpha_{IE}p_{IE}$	$\alpha_{II}p_{II}$

Table 2.4: Probability of connections in asymmetry model 2 (If asymmetry is in E to E connections,  $\alpha_{EE} = \alpha$ , and all other  $\alpha_x = 0$ )

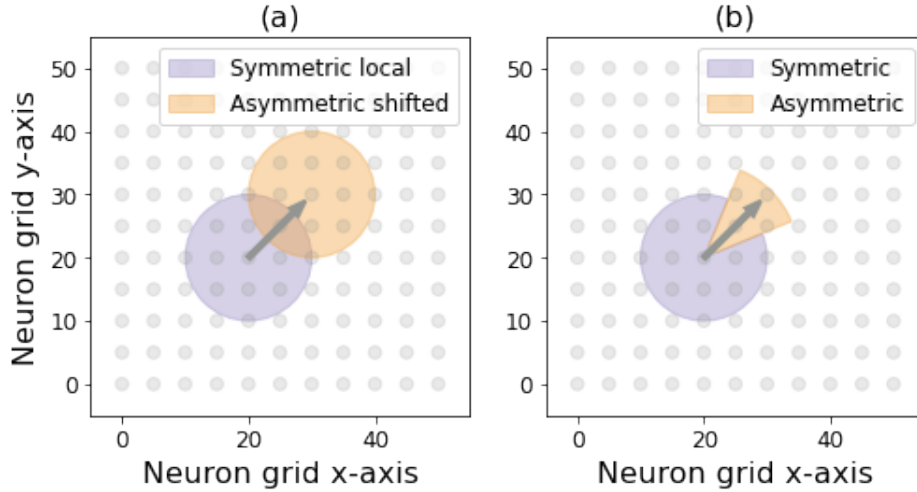


Figure 2.3: Two models of asymmetric connections.

	Excitatory	Inhibitory
Symmetric	$J$	$-gJ$
Asymmetric	$g_2J$	$-gg_2J$ (if present)

Table 2.5: Synaptic weights in model 2 of asymmetry.

### 2.3.5 Model of spatial correlation in the connectivity of neighboring neurons

Each neuron was given a value or direction of asymmetry, and these asymmetry values varied across the neuron grid. To implement spatially correlated asymmetry, we used the Perlin gradient noise which generates noise such that nearby nodes get similar values [Perlin, 1985]. Using this noise, we generated values from 0 to 7 on a  $N \times N$  neuron grid and assigned asymmetry directions according to these. The parameter 'size' determines how frequently the values change in the grid, or how spatially inhomogeneous the values in the grid are. When size = 0, the entire grid has one value. When size tends to infinity, the values are spatially random with no order. In our simulations, we used size = 3 for a 120 by 120 E neuron grid. For a given size, a random seed sets the initial conditions, which can be changed to generate many instances of the asymmetry values. These asymmetry values on a grid determine how the activity in the neuronal grid will flow. This distribution is called the 'landscape' of the network in this thesis (Figure 2.4). In this thesis, multiple

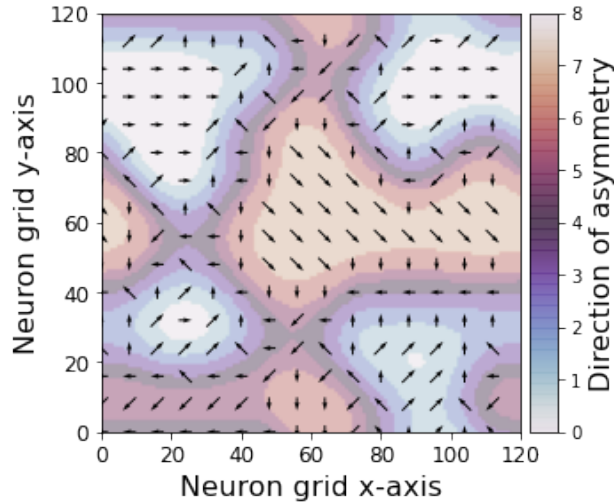


Figure 2.4: Spatial correlation in the asymmetric connections across the neuron grid. Arrows (and color) denote the direction of preferential connections. Arrows are shown at a lower resolution than color for better visibility.

landscapes refer to initialization with different initial random seed and same 'size'.

## 2.4 Input to the network

### 2.4.1 Uniform input

All neurons received a Gaussian white noise with a certain mean and standard deviation ( $\mu_{input}$  and  $\sigma_{input}$  in Equation 2.1). In results shown in this thesis, the mean was set to 400 pA and standard deviation to 100 pA.

### 2.4.2 Directed input

All neurons received a subthreshold input, and neurons in a specified region of the excitatory grid received additional suprathreshold input for 100 ms in the beginning. The subthreshold input to other neurons enables any activity to easily propagate in the net-

work. In results shown in this thesis, the subthreshold input was set to mean = 290 pA and standard deviation = 100 pA, and the additional suprathreshold input was set to mean = 700 pA and standard deviation = 0 pA. We gave this directed input to 16 regions distributed uniformly on the grid.

## 2.5 Characterizing sequences

### 2.5.1 Number of sequences

To calculate how many sequential paths can be found in a network, we considered the activity in uniform input simulations. We took the spatial positions of neurons that spike in a given time interval (10 ms). We used the algorithm DBSCAN to spatially cluster these neurons and counted the number of clusters found throughout the simulation [Ester et al., 1996]. We used clustering parameters  $\text{eps} = 3$  and  $\text{min}_{\text{samples}} = 10$  to calculate the number of activity bumps. This was kept constant across asymmetry models and type of connections, to reduce any bias.

The number of activity bumps moving around in a network is a function of the number of sequential paths and the input magnitude. Higher input can lead to multiple bumps moving on the same activity path. Because we kept the input level constant in all simulations with uniform input, the difference in number of activity bumps reflects the difference in the number of sequential paths present in the network.

To track the movement of the activity bumps, we used the method used in previous study [Spreizer et al., 2019]. We represented each spike in three dimensions, time and the spatial positions  $x$  and  $y$  of the neuron (see axes in Figure 2.5). We used DBSCAN clustering in this three-dimensional plot to track where the activity bump is moving. For this clustering to work, a suitable scaling of the time axis is required. We scaled the time axis down by a factor of 4 and used  $\text{eps} = 1.5$  and  $\text{min}_{\text{samples}} = 10$ . The clusters formed here represent each activity bump moving in time in a given direction. We found that clusters of size more than 2000 spikes in the uniform input case and 1000 spikes in the directed input case captured the activity bumps (Figure 2.5b). Smaller clusters captured random and very small sequential activity in the network (Figure 2.5a).

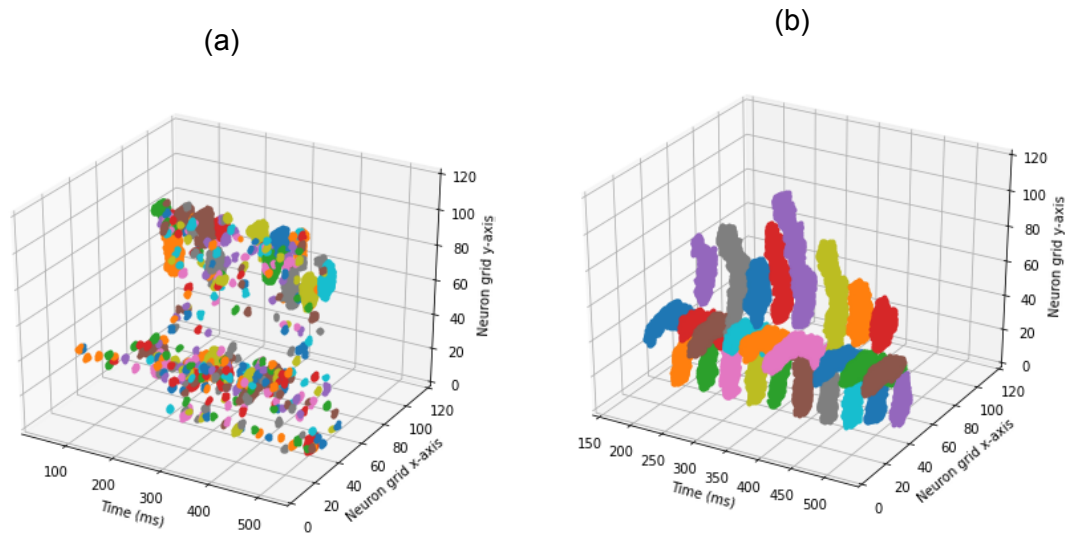


Figure 2.5: Spiketime clusters using the DBSCAN algorithm in the case of directed input. Clusters of size (a) less than 1000 points and (b) more than 1000 points

## 2.5.2 Speed of sequences

After recording moving activity bumps, we tracked the centroids of activity (in spatial axes  $x$  and  $y$ ) for each cluster and time interval. We calculated the speed of these centroids on the E neuron grid. For sequences in uniform input simulations, we took the average speed of each cluster found. For sequences evoked by directed input to multiple places in the network, we averaged the speed of the cases where activity propagates out of the initial input region.

## 2.6 Feedforward paths

### 2.6.1 Calculation of Feedforward paths

We defined a feedforward (FF) path to be the path of higher connectivity in the network. To calculate this, we used the asymmetry direction vectors of each neuron. These vectors denote the direction of preferential connections in the excitatory layer. We determined

the following possible paths through which an excitatory (E) neuron can affect another E neuron and their resultant effects:

- First-order connections:
  - E to E (excitatory effect)
- Second-order connections:
  - E to E to E (excitatory effect)
  - E to I to E (inhibitory effect)
- Third-order connections:
  - E to E to E to E (excitatory effect)
  - E to I to I to E (excitatory effect)
  - E to I to E to E (inhibitory effect)
  - E to E to I to E (inhibitory effect)

We recorded asymmetry vectors for each E neuron through every path. We had implemented spatially correlated asymmetry in different connections: from E to E, E to I, I to E, or I to I neurons; the rest were symmetric. We included multiple order connections to explain sequence formation in all these cases. When asymmetry is present in inhibitory synapses, second and third order connections are required for prediction of FF paths. As an example, suppose asymmetry is present in I to I connections. If we use only first order connections (from E to E, which are symmetric), then there is no preferred direction of excitation from each neuron and we cannot predict FF paths. Similarly, second order interactions (from E to E to E and E to I to E) do not include the asymmetry information and will suggest no preferred direction of excitation. Third order connections (through E to I to I to E) will include asymmetry information in I to I connections and give us the preferred direction of excitation at each step to predict FF paths.

We also took into account which neurons would be active by averaging over a circular or elliptical region around each point. Because only some neurons will be active, the projections by only those neurons will determine where the activity will go next.



Algorithm to calculate FF paths (Figure 2.6):

- We calculated asymmetry vectors [length, direction] for all neurons based on which direction has maximum projections. For example, we take an E neuron (index  $N_i$ ) located at  $(x_i, y_i)$  position and find the spatial positions of its postsynaptic E neurons. Then, we take the centroid of these positions, which is  $(cx_i, cy_i)$ . The vector from  $(x_i, y_i)$  to  $(cx_i, cy_i)$  is the asymmetry direction vector of neuron  $N_i$  for E to E connections. Whenever the connections are symmetric, we set the vector length and direction to zero. We calculated asymmetry vectors for first, second and third order connections by finding the postsynaptic neurons at each step and averaging the centroids of excitatory neurons at the last step. For example, to calculate second order (E to I to E) asymmetry vector from E neuron  $N_i$  at location  $(x, y)$ , we calculate  $N_i$ 's postsynaptic inhibitory neurons  $(A_0, A_1, A_2, \dots)$ . Then we find each  $A_i$ 's postsynaptic excitatory neurons  $(B_{i0}, B_{i1}, B_{i2}, \dots)$ . We take the centroid of locations of all  $B_{ij}$ 's to be  $(cx, cy)$  and record the vector from  $(x, y)$  to  $(cx, cy)$  as the second order asymmetry vector for neuron  $N_i$ .
- Initial neuron's location =  $(x_i, y_i)$
- for n steps:
  - SN = neurons surrounding point  $(x_i, y_i)$  in a circular or elliptical area
  - for all neurons in SN:
    - \* Calculate resultant excitatory vector by adding asymmetry vectors of first, second and third orders with excitatory effect and subtracting the asymmetry vectors of second and third orders with inhibitory effect.
  - $V_i$  = average of all resultant excitatory vectors of SN (weighted according to distance)
  - Next point = neuron at location  $(x_{i+1}, y_{i+1})$  which  $V_i$  points to
  - In the case of elliptical surrounding area, we tracked the tilt of ellipse and updated it using the following rule:
 
$$\text{New tilt} = 2(\text{old tilt}) + (\text{direction of } V_i)$$
- The sequence of these points  $(x, y)$  forms the FF path

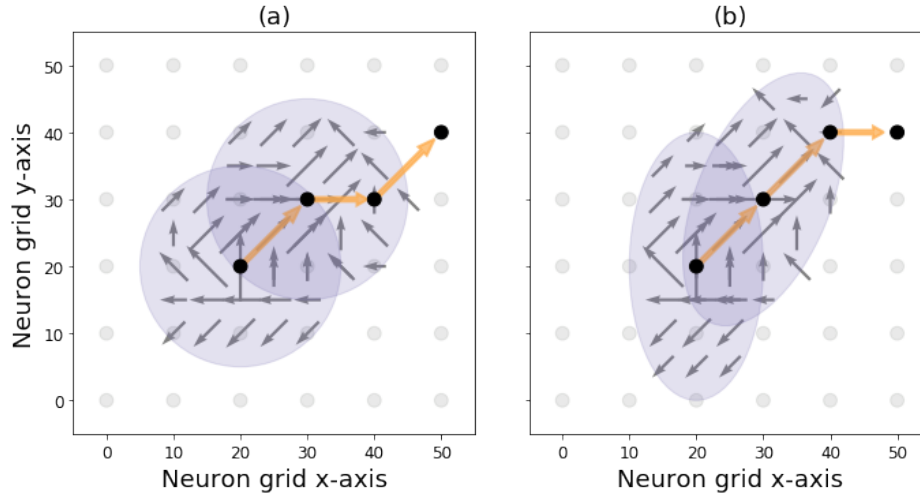


Figure 2.6: Schematic for calculation of feedforward paths by considering a weighted average of asymmetry directions over the area of activity. The next step in the path is determined by the endpoint of the averaged vector.

## 2.6.2 Comparison of anatomical feedforward paths and simulated sequential activity

We gave directed input to a region around the initial  $(x_i, y_i)$  and simulated the network for 2000 ms. We tracked the spatially localized activity in this simulation and recorded the trajectory of its centroids as the activity path. We recorded the predicted FF path from  $(x_i, y_i)$ . To compare how similar the prediction and simulated activity are, we calculated the distance between all points of FF path and activity path. For each point in the FF path, we took the minimum distance to the activity path and vice versa. We averaged these minimum distances and used it as a measure of the similarity between the predicted FF path and simulated activity path. Low distances indicate that our prediction is close to the simulation results.

## 2.6.3 Decreasing the weights of the feedforward path

We chose one region of sequences and found the corresponding predicted FF path. We found the synapses present in this FF path. To check if FF paths are indeed the cause

of sequences in this network, we reduced the weights of these synapses to zero. To compensate for the lack of synaptic input to the neurons present in this path, we increased the weight of the rest of the synapses by a certain amount. To avoid changing the structure of the rest of the network, we uniformly increased the synaptic weights of all synapses in the following way:

$$\text{Initial sum of synaptic weights} = J N_s \quad (2.4)$$

$$\text{New sum of synaptic weights} = J_{new} (N_s - N_{fs}) \quad (2.5)$$

Where,

$J$  = initial synaptic weight

$J_{new}$  = new synaptic weight

$N_s$  = number of all excitatory synapses

$N_{fs}$  = number of synapses in FF path

To conserve total synaptic input:

$$J_{new} = J \frac{N_s}{N_s - N_{fs}} \quad (2.6)$$

We first simulated a network with directed input to the region around  $(x_i, y_i)$  for 1000 ms. Then, we set the weight of FF path synapses to zero and non-FF path synapses to  $J_{new}$ . We simulated the network again with directed input to the region around  $(x_i, y_i)$  for 1000 ms. To check if the rest of the sequences are affected, we simulated the network with directed input to a different sequence generating region around  $(x_j, y_j)$  for 1000 ms. Then, we compared the number of activity bumps formed in these cases.

## 2.7 Search for background activity state

### 2.7.1 Globally random connections

Spatially correlated asymmetry generates sequences starting from a very low threshold. To make the network more likely to sustain background activity, we added spatially random

connections into the network. For this, half of the connections were wired according to spatially correlated asymmetry (Model 1 of asymmetry), and the other half were random global connections. The strength of connections was varied according to the parameters in Tables 2.6 and 2.7.

	Excitatory	Inhibitory
Random global connections	$J$	$-gJ$
Asymmetric local connections	$g_2J$	$-gg_2J$

Table 2.6: Synaptic weights distribution in partially random networks

Parameter	Value
$g$	8
$J$	10
$g_2$	2

Table 2.7: Initial synaptic weight parameters in partially random networks

## 2.7.2 Parameter search with different input levels

If a network supports background activity state, it should show spatially random activity at low input levels and sequential activity at high input levels. Using the above network, we simulated multiple parameter combinations with different input levels to check if this separation was present.

## 2.7.3 Parameter search with increasing and decreasing values

Apart from a parameter sweep, we also used a different approach of varying parameters serially. For each parameter in the list (Table 2.8), we increased the value of this parameter (say  $A$ ) in steps. For each value of parameter  $A$ , we simulated the network for 1000 ms and then changed the value of  $A$  to the next value. For each value of  $A$ , after the network reaches a stable state, we recorded the sequential activity state by counting the number of activity bumps present in the last 100 ms. We simulated the network with increasing

and decreasing value of  $A$  in a given range and checked the presence of hysteresis in the number of activity bumps. If hysteresis is present for some value of  $A$ , it implies that two network states are possible in that parameter condition.

Parameter	Value range
Network input	200 to 700 in steps of 50
Probability of E to E connections ( $p_{EE}$ )	0.04 to 0.05 in steps of 0.002
Inhibition to excitation ratio ( $g$ )	5 to 15 in steps of 1
Synaptic strength ( $J$ )	5 to 25 in steps of 2.5

Table 2.8: List and range of values for serial parameter search for background activity state



# Chapter 3

## Results

Here we investigate the emergence of sequential firing of neurons in a locally connected random network of excitatory and inhibitory neurons (EI-LCRN network). Specifically, we are interested in understanding how spatial correlations in different types of recurrent connections affect the properties of sequential activity and to what extent the network structure predicts the neuronal activity sequences.

### **3.1 Sequential activity in networks with correlated spatial asymmetry in EI and IE connections**

Previously, [Spreizer et al., 2019] showed that in an EI network spatially correlated asymmetric connections of individual neurons lead to spatiotemporal sequences of neuronal activity. Similarly, in a purely inhibitory network sequences emerge when the recurrent inhibitory neurons are wired with spatially correlated asymmetry. However, it is not clear if in an EI-LCRN, connection asymmetry in inhibitory to excitatory (IE) or excitatory to inhibitory (EI) can also generate sequential activity. We simulated EI-LCRN (Figure 2.1) similar to previous study [Spreizer et al., 2019]. We implemented spatially correlated asymmetry individually in either E to E, E to I, I to E and I to I connections (will be denoted as EE, EI, IE and II connections). We found that spatio-temporal sequences can be formed with any

of these asymmetries (Figure 3.1). We detected the presence of sequences by counting

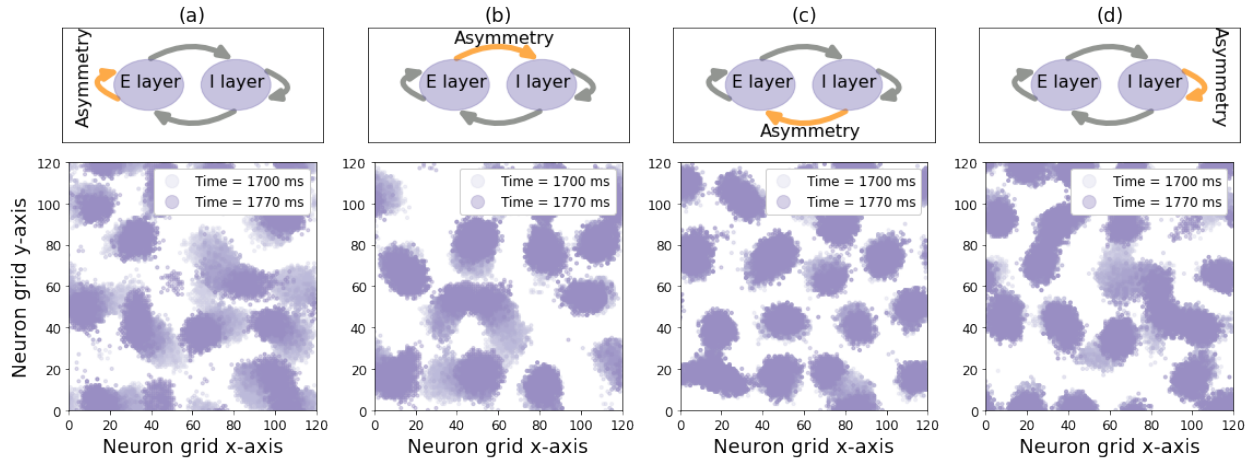


Figure 3.1: Sequential activity when spatially correlated asymmetry is present in connections from (a) E to E, (b) E to I, (c) I to E, and (d) I to I neurons. Low and high intensity of color in the plots determines activity in different time points.

the number of localized activity regions or bumps using DBSCAN, a clustering algorithm (Methods 2.5). The number of activity bumps is a readout of the number of sequential paths present in the network. The average number of activity bumps for each type of connection asymmetry is shown in Figure 3.2. We also compared the speed of each activity bump as a measure of speed of sequences in the network for the different configurations (Figure 3.2). While the number of sequential paths was similar in all asymmetry cases, speed of sequences was much lower in the IE and II asymmetry case. These results confirm that as long as correlated connection asymmetry exists in the connection of excitatory or inhibitory neurons, EI-LCRN can exhibit sequential activity.

### 3.2 Second model of asymmetry which includes symmetric connections also generates sequences

In a biological network, connections from one layer to another can happen through multiple channels, and asymmetric and symmetric connections can be simultaneously present. Therefore, we implemented a different model of asymmetry where both symmetric and



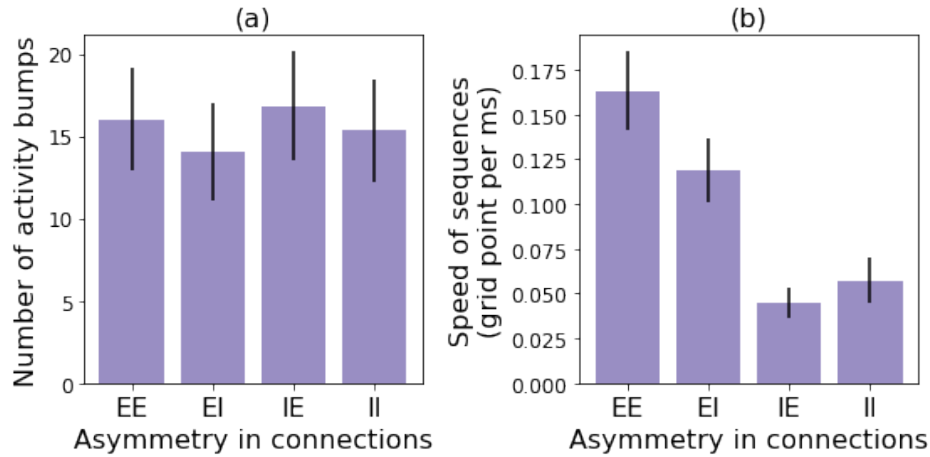


Figure 3.2: (a) Number of sequential paths and (b) speed of sequences on the neuron grid when spatially correlated asymmetry is present in different connections. The number and speed values are averaged over 10 trials for 20 different connectivity landscapes. Error bar denotes the standard deviation across landscapes

asymmetric connections can be included (Figure 2.3, Methods 2.3.4). Spatial correlation in this second model of asymmetry also generates spontaneous sequences. Again, spatially correlated asymmetry in any connections (EE, EI, IE, and II) gave rise to sequential activity (Figure 3.3). As a higher spatial spread of connections was used in this case (Table 2.3), the activity bumps created were larger in size compared to activity bumps formed using model 1 of asymmetry (Figure 3.1). In some cases of asymmetry in E to E connections, we observed the shape of the localized activity to be elliptical (Figure 3.4). In the rest of the cases, the shape of the localized activity is circular (Figure 3.3 and 3.4). We presume that elliptical activity bumps arise due to extended connectivity in one direction. We also observed that sequential paths with elliptical bumps were much more spatially defined and separated. Similar to the first model of asymmetry, we observed a similar number of bumps for different types of connection asymmetries (Figure 3.5). However, with this connectivity model, the speed of sequences was smaller when connection asymmetry was in EI and IE connections.

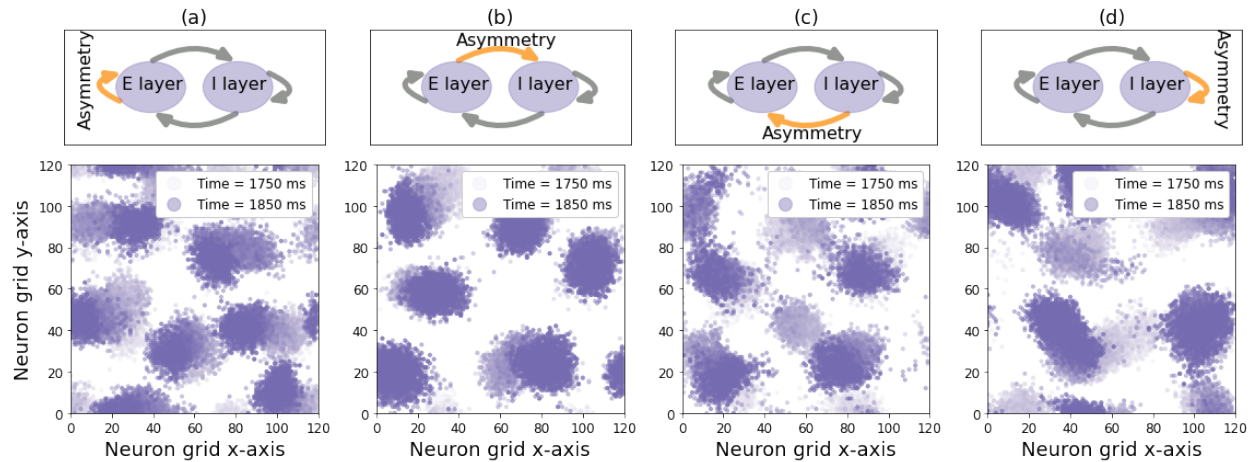


Figure 3.3: Sequential activity when spatial correlation is implemented using the second model of asymmetry in connections from (a) E to E, (b) E to I, (c) I to E, and (d) I to I neurons

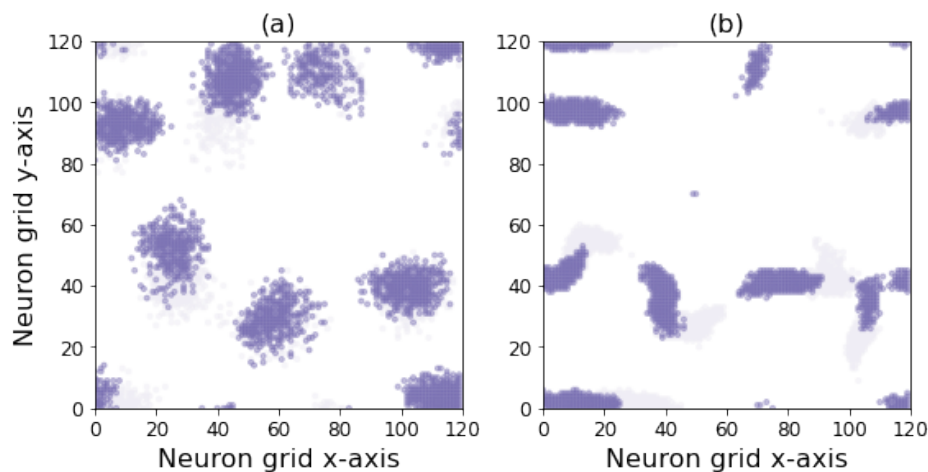


Figure 3.4: Shapes of neural activity localization when spatially correlated asymmetry is present in E to E connections with different levels of relative asymmetry. (a) Low relative asymmetry causes circular activity regions, (b) Higher relative asymmetry causes elliptical activity regions.

### 3.3 State transition to stationary activity due to relative strength of asymmetry

We found that in certain parameter regimes, the second model of asymmetry gave rise to spatially constricted stationary activity (Figure 3.6), that is bump speed was reduced

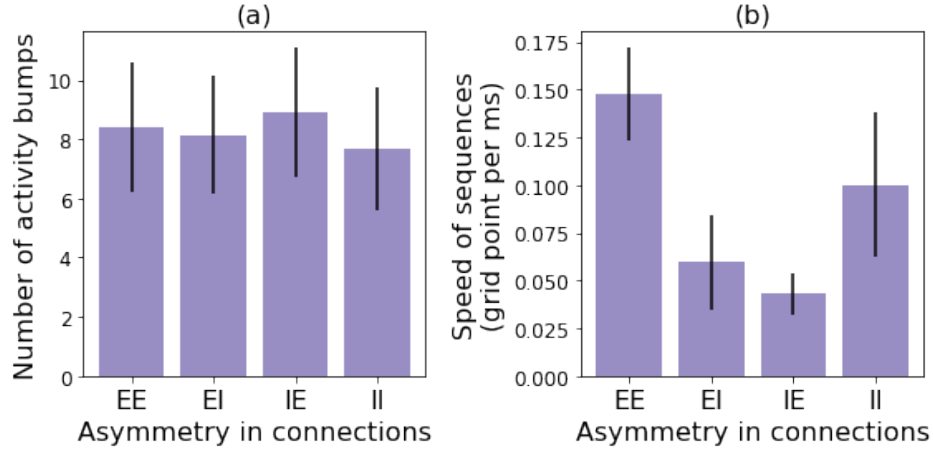


Figure 3.5: (a) Number of sequential paths and (b) speed of sequences on the neuron grid when spatially correlated asymmetry (second model) is present in different connections. The number and speed values are averaged over 10 trials for 20 different connectivity landscapes. The error bar denotes standard deviation across landscapes.

to zero. This dynamical state is similar to the k-winner-take-all solution often observed in LCRNs [Roxin et al., 2005]. We found the following parameters to be important for this state transition:

- Relative number of asymmetric to symmetric synapses =  $\alpha$
- Relative strength of asymmetric to symmetric synapses =  $g_2$

We simulated EI-LCRNs with a range of these two parameters and calculated the speed of localized activity. Speed of sequences can be used as a proxy for sequential or stationary activity. When speed is high, the network has moving localized activity. When speed is near zero, the network either has no localized activity or the localized activity is stationary in the grid. We draw a phase plot of the network's behavior relative to the above parameters with asymmetry in different connections (Figure 3.7). Interestingly, the transition to stationary bumps state occurred for different ranges of  $\alpha$  and  $g_2$  in the four connection asymmetry configurations. We observe that when asymmetry is in EE connections, higher asymmetry gives faster sequences. However, when the asymmetry is in EI, IE and II connections, an intermediate alpha is required for formation of sequences.

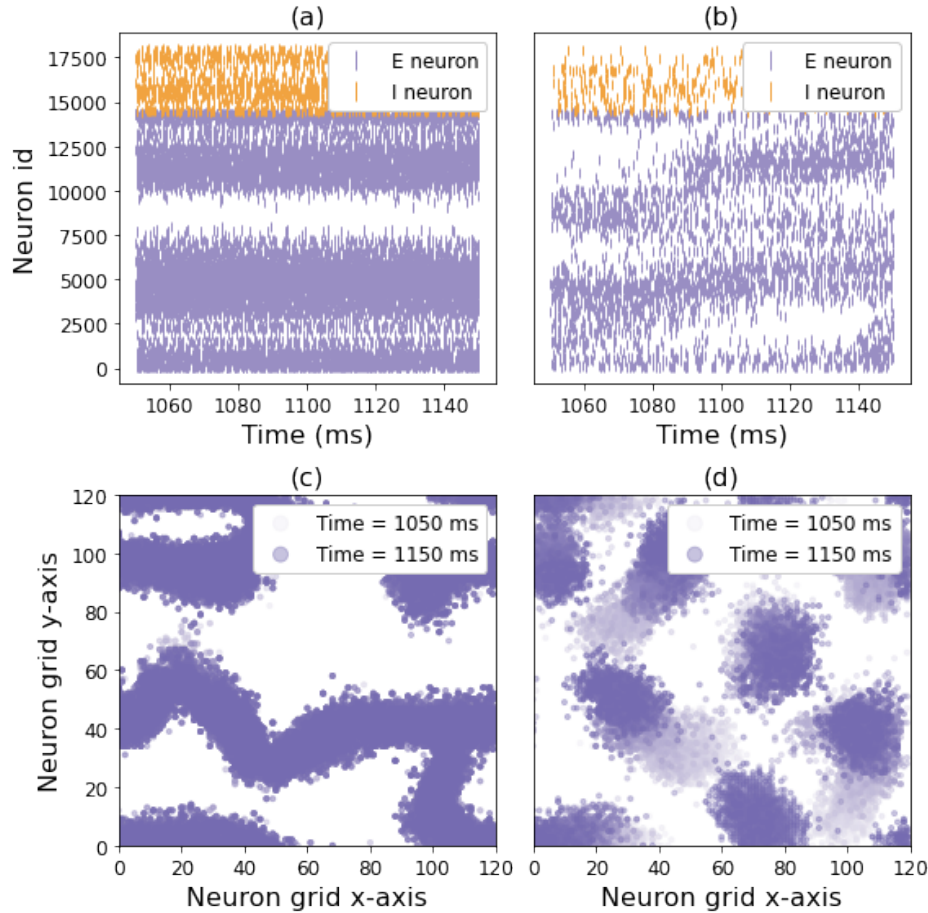


Figure 3.6: Example raster plots and spatial network activity of (a), (c) stationary and (b), (d) sequential activity formed by different amounts of relative asymmetry. The cases shown here are for asymmetry in E to E connections. Stationary activity has  $g_2 = 2.5$ ,  $\alpha = 0.1$  and sequential activity has  $g_2 = 1$ ,  $\alpha = 0.1$  (see values in phase plot Figure 3.7).

### 3.4 Embedded feedforward paths predict sequences

Why does such correlated asymmetric connectivity give rise to sequential activity? [Spreizer et al., 2019] already indicated that such connectivity schemes result in formation of feedforward pathways in EI-LCRNs when connection asymmetry exists in EE connections. However, it is not clear if the same argument can be extended to connection asymmetry in EI and IE connections. We hypothesized that underlying paths of higher connectivity or feedforward (FF) paths are the mechanism of sequences in this model. To test this, we checked if FF paths can be found in different asymmetry configurations and if they pre-

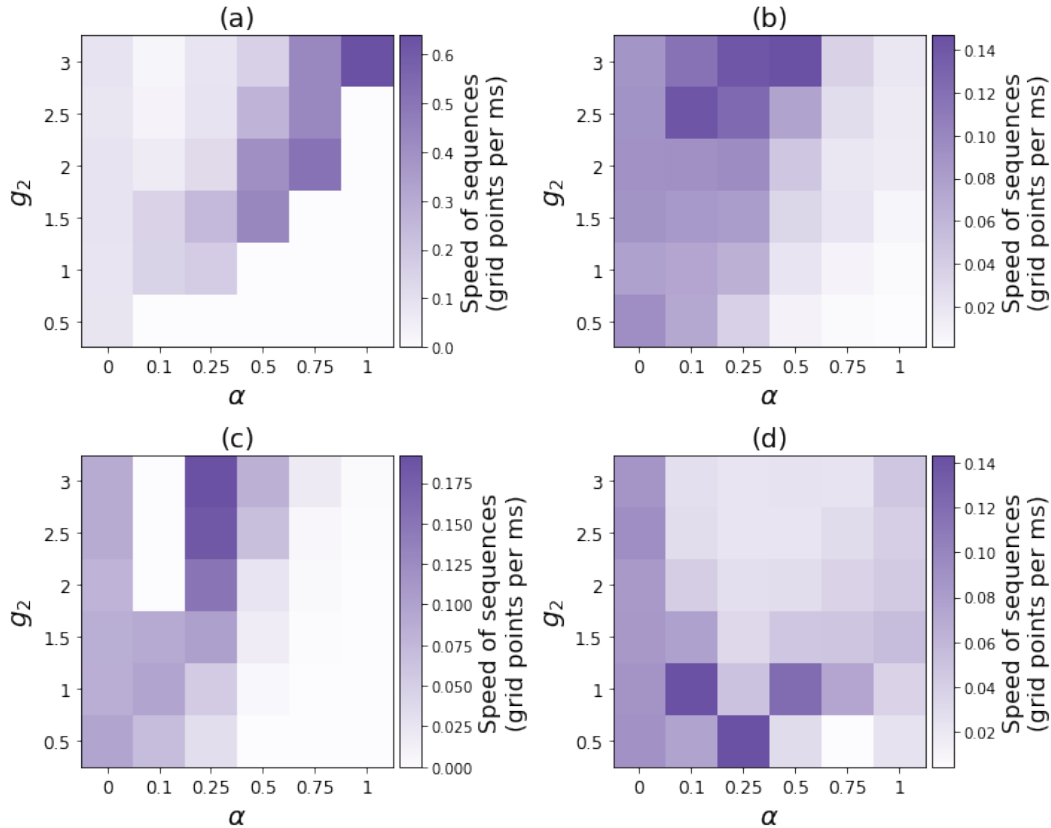


Figure 3.7: Phase plot of change in network dynamical state as a function of relative asymmetry. X-axis and y-axis are the relative number and strength of asymmetric connections respectively. Spatially correlated asymmetry was present in (a) E to E, (b) E to I, (c) I to E, and (d) I to I connections. Color in the heatmap denotes the speed of localized activity averaged over 5 different landscapes.

dict the sequences that arise in simulations. We estimated the path of high connectivity from a given location  $(x, y)$  in the network (Methods 2.6). For each network, we did this for 16 different locations uniformly distributed in the network. For each of these locations, we simulated the network with directed input to an 8 by 8 region in the neuron network around this location (Figure 3.8). Next, we compared the similarity between predicted FF path and simulated activity path by calculating the distance between the two paths for different asymmetry configurations (Figure 3.9). We found that FF paths formed by adding excitatory and subtracting inhibitory connectivity directions can predict the path taken by sequential activity, as reflected by small distances ( $< 5$  grid points) between the predicted and simulated activity paths. When the activity bump is large and elliptical, it is important

to include the shape of the activity bump to predict these sequences (Figure 3.8(e,j)).

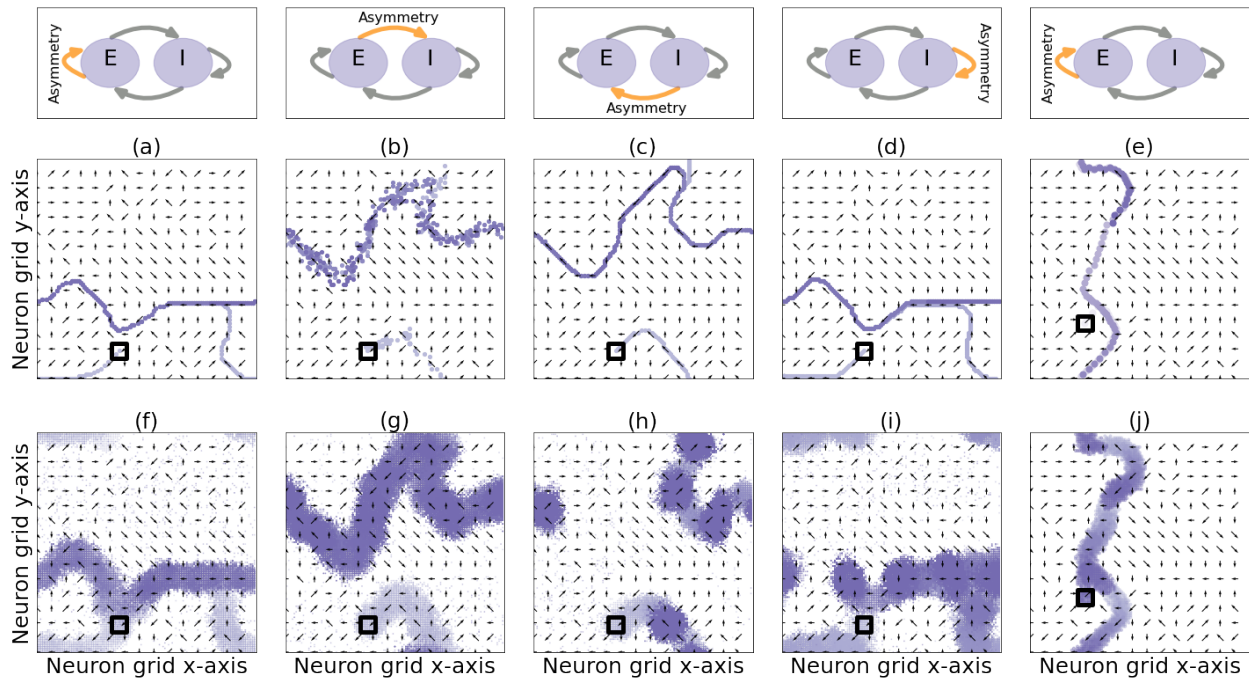


Figure 3.8: Examples of predicted feedforward paths (a,b,c,d,e) and corresponding simulated activity path (f,g,h,i,j) starting from the same point (denoted by black square). (a,f): (a) Anatomical FF path and (f) simulated activity sequence when spatially correlated asymmetry was present in E to E connections wired using model 1 of asymmetry. (b,g): Same as in (a,f) but when spatially correlated asymmetry was present in E to I connections (c,h): Same as in (a,f) but when spatially correlated asymmetry was present in I to E connections (d,i): Same as in (a,f) but when spatially correlated asymmetry was present in I to I connections (e,j): Same as in (a,f) but when spatially correlated asymmetry was present in E to E connections using model 2 of asymmetry with elliptical activity bumps. Black square denotes origin of predicted FF path and the location of directed input in simulated activity path. The landscape, identical in all plots, is the same as in Figure 2.4.

### 3.5 Silencing embedded feedforward paths reduces the sequences

We next asked if silencing FF paths prevents the spatiotemporal sequences from being generated to establish a causal relationship between anatomical FF paths and neuronal

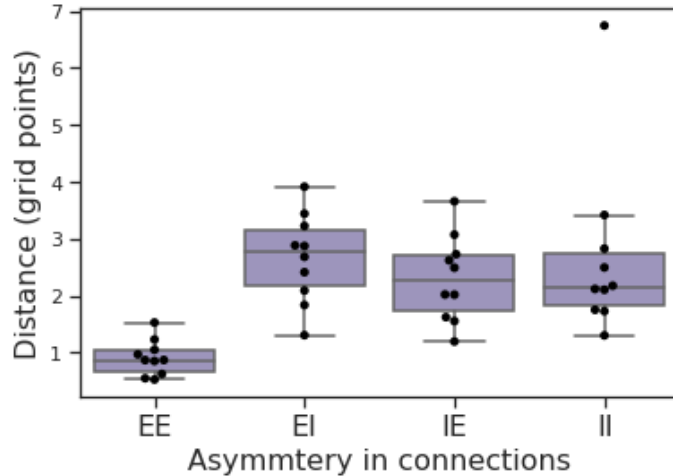


Figure 3.9: Distance between predicted feedforward paths and simulated activity path, when asymmetry is present in different connections using Model 1 of asymmetry. Values of distances are averaged over 16 positions for each of the 10 different landscapes.

activity sequences. To answer this, we simulate a network in sequence generating state for 1000 ms. Then we reduce the synaptic weights of FF path synapses to zero (Figure 3.10) and continue to simulate the network for 1000 ms. Then, we simulate the network again for 1000 ms giving directed input to another sequence generating region to check if other sequences are affected. The number of sequences in these configurations of the simulation when asymmetry is in EE connections using model 1 of asymmetry are compared in Figure 3.11. Reducing the weights of FF paths impairs the number of sequences present in that region. We also observed that only the reduced synaptic weights path is affected; sequences in other regions remained intact.

### 3.6 Spatially random background activity state

We asked if this network can sustain a state with spatially random background activity along with a sequential activity state. We aimed to achieve a state in which different input configurations (high or low, uniform or directed) can give rise to either background activity or sequential activity, without having to change the synaptic weights distribution of the network. On trying multiple parameter sweeps, we found that it was non-trivial to have

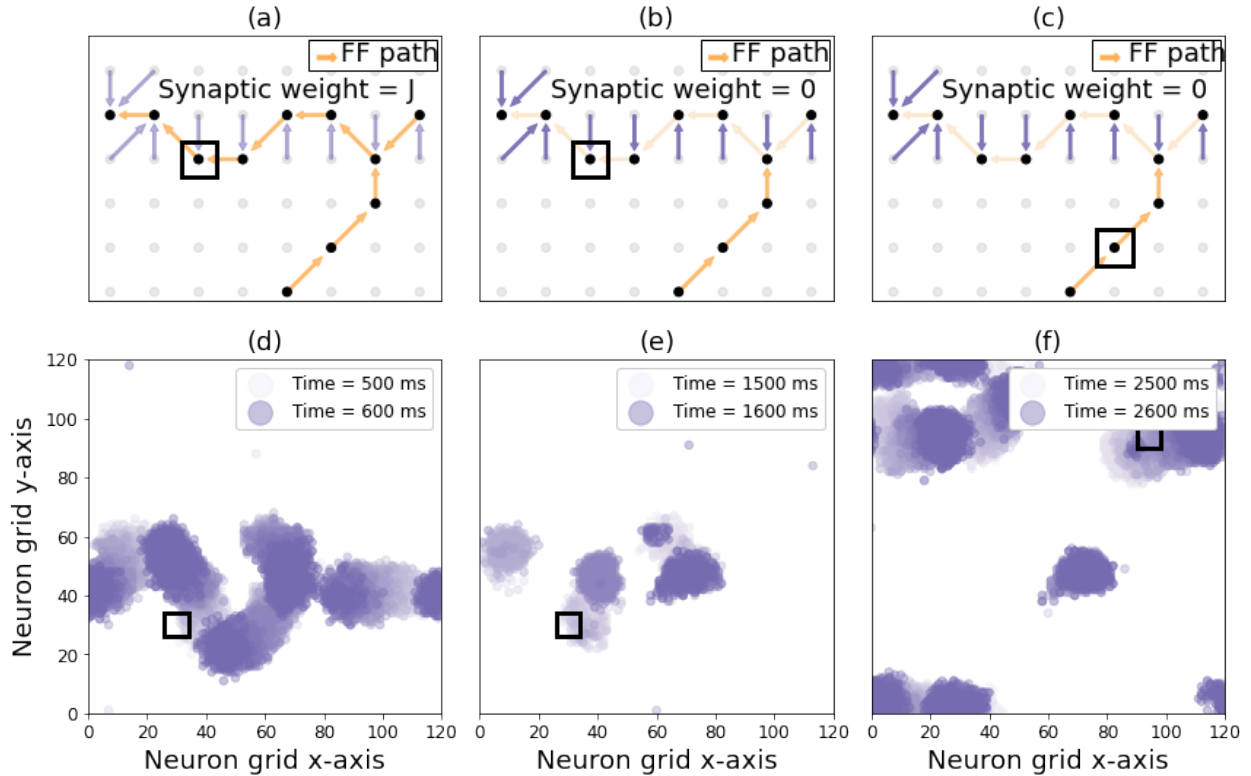


Figure 3.10: Schematic for simulation with reduced synaptic weights for the FF path. (a) before and (b), (c) after reduction of weights. Examples of neural activity (d) before and (e), (f) after reduction of FF path synaptic weights. The black square in all plots marks the region of directed input. The black square in (a,b,d,e) marks the location  $(x_i, y_i)$  from where the FF path was calculated.

two different activity states simultaneously in the network. Once the synaptic weights and connectivity profile is specified, the network dynamics is limited to one of the two desired states. Alternatively, we tried to change certain parameters incrementally in one simulation (Methods 2.7). We tried a series of values for some parameters in increasing and decreasing order and recorded the network activity state (as the number of activity bumps) for each value. We found that for parameters that could be changed on the fly in a simulation (Table 2.8), most do not lead to multiple network states (Figure 3.12).



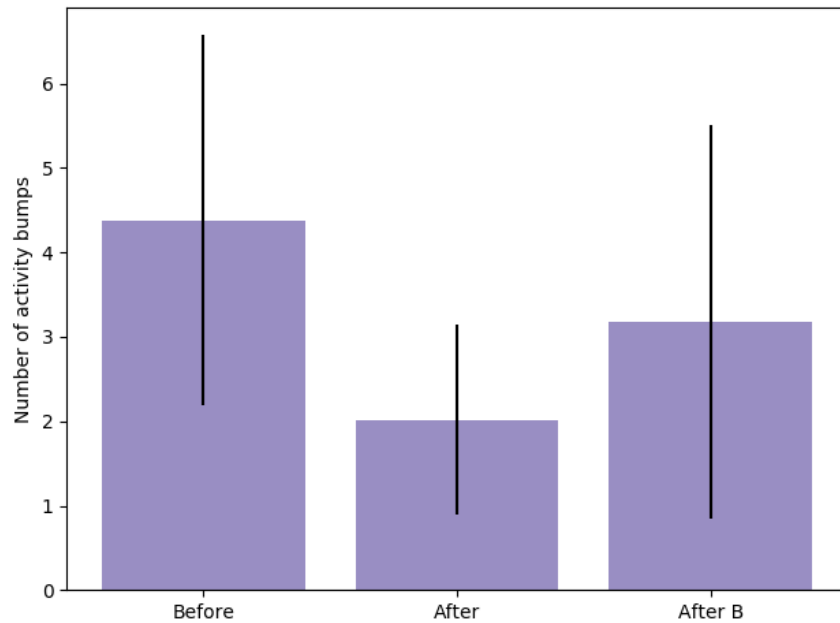


Figure 3.11: Number of sequences formed 'Before' and 'After' the reduction of FF path (from region A) synaptic weights, directed input was given to region A. 'After B' denotes the part of simulation after reduction of FF path synaptic weights, when directed input given to another sequence generating region B. Number of bumps are averaged over simulations in 5 different landscapes where spatially correlated asymmetry (model 1) was present in E to E connections

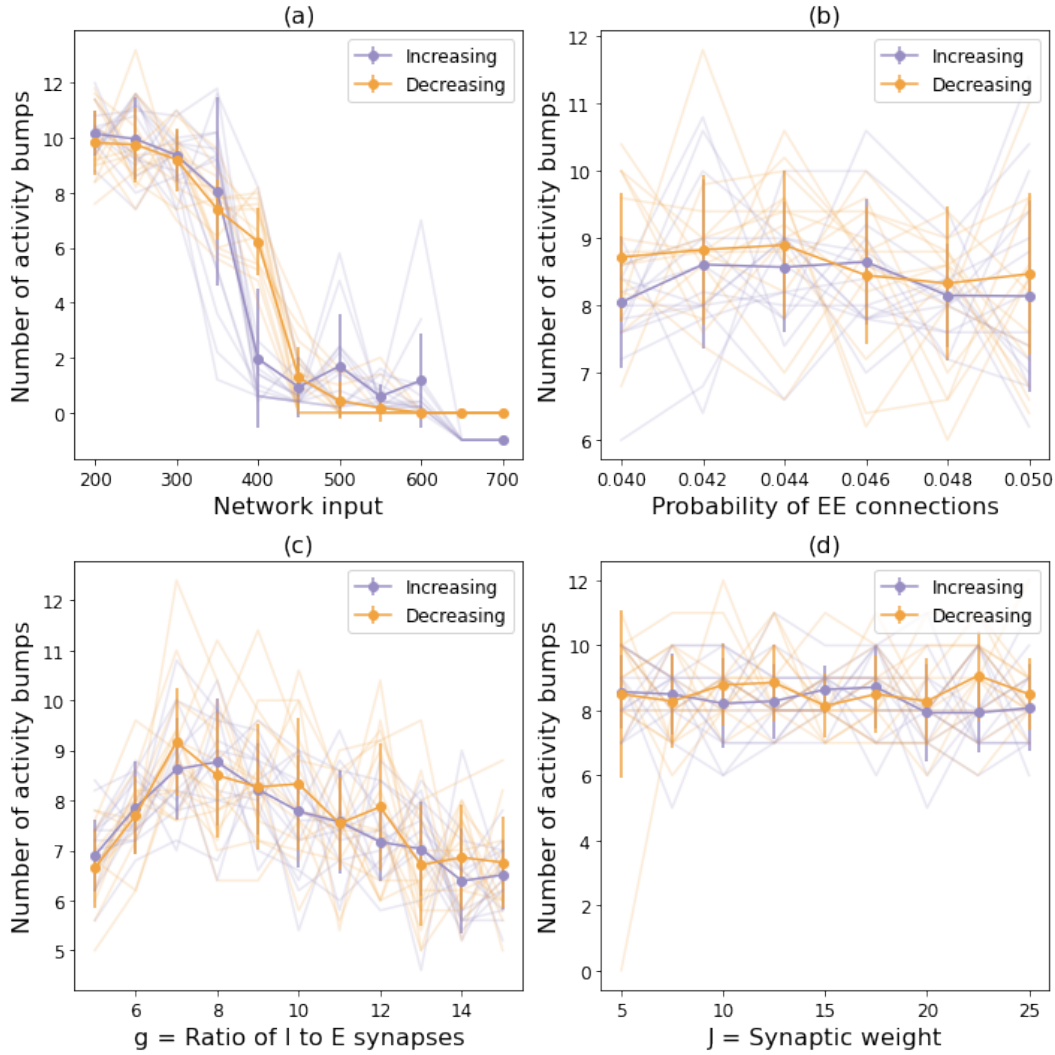


Figure 3.12: Number of activity bumps formed in a simulation as a proxy for network activity states when parameter  $A$  on the x-axis is varied in increasing and decreasing orders. Lighter traces show individual trials. Darker traces show the average number of activity bumps across trials. Different parameters on x-axis are (a) Magnitude of network input ( $\mu_{input}$  in Equation 2.1), (b) probability of recurrent excitatory connections  $p_{EE}$ , (c) Excitatory synaptic weight  $J$ , and (d) the ratio of inhibition to excitation  $g$  (see Table 2.8).

# Chapter 4

## Discussion

Reliable sequential activation of neurons is necessary for animal behavior. Trivially, sequential activity of neurons can be a simple consequence of external input. However, sequential activity is observed in cognitive tasks where there is no explicit ordered stimulus. Therefore it is important to identify mechanisms that can give a network ability to generate sequences intrinsically. Given their importance, a number of models have been proposed to explain the emergence of sequential activity of neurons. But all those mechanisms rely on supervised learning or manual wiring of connectivity in a specific manner. In this work we investigate how a simple and biologically plausible generative rule can wire the network in such a way to embed effective feedforward pathways which provide the necessary structural substrate to generate reliable sequential activity. Our rule modifies the projection region of each neuron by either shifting it or increasing the number of post-synaptic neurons in a certain direction. We do this in a spatially correlated manner across the network, such that spatially closer neurons have their projections regions shifted or increased in similar directions.

## **4.1 Mechanism for sequences when spatially correlated asymmetry is present in EI, IE and II connections.**

When asymmetry is present in recurrent excitatory connections, it is straightforward how sequences are formed: each neuron projects to a certain direction and its nearby neurons also project to the same region. This forms paths of higher connectivity, which is followed by sequential neural activity.

However, in the case of asymmetry in the other connections (EI, IE, and II), the mechanism of sequential activity is not straightforward. As we have shown in this work, correlated asymmetry in EI, IE and II connections can also generate sequential activity. Here we propose a possible mechanism that underlies emergence of sequential activity in networks with correlated asymmetry in EI, IE and II connections. Any activity in the excitatory (E) layer, causes activity in the inhibitory (I) layer which gives wider feedback inhibition to the E layer, thus localizing the E layer activity.

- When asymmetry is in E to I connections, the region of the I layer that gets activated is shifted from the original position of activity on the E layer. Therefore, the feedback inhibition to the E layer is also shifted in the direction of the asymmetry vector. Due to recurrent E connections, net excitation in the E layer is shifted opposite to the asymmetry vector directions and activity propagates in this path.
- When asymmetry is in I to E connections, the region in the I layer that gets activated is the same, but the inhibition from I to E layer shifts in asymmetry vector direction. Therefore, feedback inhibition to the E layer is shifted and net excitation is opposite to the asymmetry vector direction, which is followed by the activity path.
- When asymmetry is in I to I connections, the region of the I layer activated by the E layer is the same. As recurrent inhibition is higher in one direction, the active region in the I layer shifts to the direction opposite of the asymmetry vector. The inhibition from I layer to E layer is shifted opposite to the asymmetry vector directions, and the net excitation follows the original asymmetry directions.

As the directional activity has to go through multiple layers in these cases, the speed of sequences is lower than when asymmetry is in recurrent excitatory connections.

## **4.2 Feedforward paths based on connectivity can be used to predict sequences**

Feedforward connectivity in a network is either manually built into models of sequences generation or it is created through learning. Here, we have shown that there is another way of generating feedforward paths in a network by changing the projection regions of neurons in a spatially correlated manner. Our results prove that paths of higher net excitation are the underlying mechanism of sequences in these networks. We have suggested a method of relating the underlying connectivity to the order of neurons firing in a sequence. This result opens the possibility of predicting which neurons will be part of a sequence in biological networks if certain patterns of the underlying connectivity can be obtained.

## **4.3 Different states in new model of asymmetry**

We observed that by changing the relative amount of asymmetry in the system using model 2 of asymmetry, the network can shift between moving and stationary localized activity states. For example in the case of EE asymmetry, higher and stronger asymmetric connections make faster sequences. In the case of EI, IE and II asymmetry, an intermediate number of asymmetric connections is required. We also observed that whenever stationary activity is found, it does not localize spatially into circular or elliptical bumps. Rather, it localizes into larger regions without any particular shape (Figure 3.6).

When asymmetry is in EE connections, higher asymmetry forms more distinct FF paths and therefore, the likelihood of sequential activity increases with the amount of asymmetry. When asymmetry is in EI, IE and II cases, both higher and lower numbers of asymmetric

connections are detrimental for the movement of activity. In these cases, asymmetry goes through the feedback inhibition from the I layer. This inhibition is also responsible for the localization of activity into smaller bumps. Therefore, we suggest that when the number of asymmetric connections is very high, the spatial spread of inhibition is insufficient to localize the E layer neural activity into a bump. This results in large regions of active E neurons with no net direction of higher excitation and we observe the stationary activity state. When the number of asymmetric connections is very low, the push for directional motion is not enough and we observe random activity. We can further speculate that if projection regions of inhibition are larger or the spatial spread of I to E connections is increased, sequences can be formed in some of the regions where we currently observe the stationary localized activity states.

The importance of this result lies in the demonstration of the effect of the spatial distribution of inhibitory input on a sequential network state. We have shown that for sequences to be present in a network, the inhibitory synapses need to be distributed appropriately for the network to show non-stationary activity.

## **4.4 Importance of spatial localization for sequential activity**

There are two important dynamical phenomena in this model: localization and movement of neural activity. From previous work on the model, we know that spatially correlated asymmetry generates the movement of activity. In this work, we prove that the underlying asymmetry landscape causes the movement of neural activity through the formation of FF paths.

In light of our results, we can comment on the importance of localization of activity. Spatial localization of activity into small defined regions (like circles or ellipses) arises due to local recurrent connections and feedback inhibition. Recurrent connections are cru-

cial for the propagation of sequences by forming FF paths. They also control the shape of spatial localization; elliptical activity regions are only formed when the second model of asymmetry is used in recurrent excitatory connections. Different shapes of spatial localization can change the FF paths formed, even if the underlying landscape remains identical. We also observed that appropriate inhibition is required for spatial localization and a change in this inhibition can lead to loss of sequential activity.

When neural activity gets organized into smaller regions of activity, the active region has a significant net excitation in a certain direction that arises from the underlying landscape. Only when this significant excitation in a particular direction is present, the neural activity will move in that direction. When activity gets localized into large regions, the net excitation is not significant and directional for the active region to move. Thus, appropriate spatial localization is also crucial for the generation of sequences in this model.

Therefore, we conclude that recurrent connections and feedback inhibition in an EI network would be prerequisite biological properties for this kind of sequence generation. Additionally, the localization of neural activity to certain groups of neurons would be an important phenomenon co-occurring with these kind of sequences.

## **4.5 Spatial structure of the network and background activity state**

We assume that an underlying spatial structure is present in neural networks. Local connections, spatial localization of activity and spatially correlated asymmetry, all depend on the arrangement of neurons on a two-dimensional grid. However, this arrangement is unlikely to be true for a biological network. While some proof of global connectivity patterns are present, spatially patterned activity has rarely been observed in biological network recordings that contain both network activity and spatial position of neurons (for example calcium imaging recordings). We can hypothesize that biological networks have a struc-

ture similar to our model, but the biological spatial positions of the neurons are jumbled up. However, we must compare the underlying structure of the biological network to our model. In this work, we aimed to do this by comparing the background activity states of the biological and model network. For this study, we defined background activity state to be a spatially random activity state induced by low magnitude non-patterned input.

To induce a background activity state in our model, we need to prevent the spatial localization of neural activity. We found that transient activation and inactivation of spatial localization is unfeasible in most of the parameter space of our model. We varied the factors that affect spatial localization (recurrent connections, inhibitory synaptic weights, etc) and observed that most parameter combinations do not support a distinct background activity state in these networks. We continue to check more parameters to rule out any other possible cases. It is possible that a very fine balance of synaptic weights leads to a network state that exhibits both the desired states. If it is entirely impossible to have simultaneous background and sequential activity state in the model, then we would need another way to relate the connectivity structure of biological networks to our model.



# References

- [Abeles, 1991] Abeles, M. (1991). *Corticonics: Neural circuits of the cerebral cortex*. Cambridge University Press.
- [Azizi et al., 2013] Azizi, A. H., Wiskott, L. and Cheng, S. (2013). A computational model for preplay in the hippocampus. *Frontiers in Computational Neuroscience* 7.
- [Bakhurin et al., 2017] Bakhurin, K. I., Goudar, V., Shobe, J. L., Claar, L. D., Buonomano, D. V. and Masmanidis, S. C. (2017). Differential Encoding of Time by Prefrontal and Striatal Network Dynamics. *The Journal of neuroscience : the official journal of the Society for Neuroscience* 37, 854–870.
- [Bernard and Wheal, 1994] Bernard, C. and Wheal, H. V. (1994). Model of local connectivity patterns in CA3 and CA1 areas of the hippocampus. *Hippocampus* 4, 497–529.
- [Bhalla, 2019] Bhalla, U. S. (2019). Dendrites, deep learning, and sequences in the hippocampus. *Hippocampus* 29, 239–251.
- [Bouchard and Brainard, 2016] Bouchard, K. E. and Brainard, M. S. (2016). Auditory-induced neural dynamics in sensory-motor circuitry predict learned temporal and sequential statistics of birdsong. *Proceedings of the National Academy of Sciences* 113, 9641–9646.
- [Diesmann et al., 1999] Diesmann, M., Gewaltig, M.-O. and Aertsen, A. (1999). Stable propagation of synchronous spiking in cortical neural networks. *Nature* 402, 529–533.
- [Dragoi and Buzsáki, 2006] Dragoi, G. and Buzsáki, G. (2006). Temporal Encoding of Place Sequences by Hippocampal Cell Assemblies. *Neuron* 50, 145–157.
- [Dragoi and Tonegawa, 2011] Dragoi, G. and Tonegawa, S. (2011). Preplay of future place cell sequences by hippocampal cellular assemblies. *Nature* 469, 397–401.
- [Ester et al., 1996] Ester, M., Kriegel, H.-P., Sander, J. and Xu, X. (1996). A density-based algorithm for discovering clusters in large spatial databases with noise. pp. 226–231, AAAI Press.

- [Goudar and Buonomano, 2015] Goudar, V. and Buonomano, D. V. (2015). A model of order-selectivity based on dynamic changes in the balance of excitation and inhibition produced by short-term synaptic plasticity. *Journal of Neurophysiology* 113, 509–523.
- [Haga and Fukai, 2018] Haga, T. and Fukai, T. (2018). Recurrent network model for learning goal-directed sequences through reverse replay. *eLife* 7, e34171.
- [Hahnloser et al., 2002] Hahnloser, R. H. R., Kozhevnikov, A. A. and Fee, M. S. (2002). An ultra-sparse code underlies the generation of neural sequences in a songbird. *Nature* 419, 65–70.
- [Harvey et al., 2012] Harvey, C. D., Coen, P. and Tank, D. W. (2012). Choice-specific sequences in parietal cortex during a virtual-navigation decision task. *Nature* 484, 62–68.
- [Hebb, 1949] Hebb, D. O. (1949). The organization of behavior; a neuropsychological theory. *The organization of behavior; a neuropsychological theory.*, Wiley, Oxford, England. Pages: xix, 335.
- [Ishizuka et al., 1990] Ishizuka, N., Weber, J. and Amaral, D. G. (1990). Organization of intrahippocampal projections originating from CA3 pyramidal cells in the rat. *The Journal of Comparative Neurology* 295, 580–623.
- [Itskov et al., 2011] Itskov, V., Curto, C., Pastalkova, E. and Buzsáki, G. (2011). Cell assembly sequences arising from spike threshold adaptation keep track of time in the hippocampus. *The Journal of neuroscience : the official journal of the Society for Neuroscience* 31, 2828–34.
- [Krofczik et al., 2009] Krofczik, S., Menzel, R. and Nawrot, M. P. (2009). Rapid odor processing in the honeybee antennal lobe network. *Frontiers in Computational Neuroscience* 2.
- [Kumar et al., 2008] Kumar, A., Rotter, S. and Aertsen, A. (2008). Conditions for Propagating Synchronous Spiking and Asynchronous Firing Rates in a Cortical Network Model. *Journal of Neuroscience* 28, 5268–5280.
- [Lashley, 1951] Lashley, K. S. (1951). *The problem of serial order in behavior*, vol. 21., Bobbs-Merrill Oxford, United Kingdom.
- [Mazor and Laurent, 2005] Mazor, O. and Laurent, G. (2005). Transient Dynamics versus Fixed Points in Odor Representations by Locust Antennal Lobe Projection Neurons. *Neuron* 48, 661–673.
- [Modi et al., 2014] Modi, M. N., Dhawale, A. K. and Bhalla, U. S. (2014). CA1 cell activity sequences emerge after reorganization of network correlation structure during associative learning. *eLife* 3.

- [Murray and Escola, 2017] Murray, J. M. and Escola, G. S. (2017). Learning multiple variable-speed sequences in striatum via cortical tutoring. *eLife* 6, e26084.
- [Muto et al., 2013] Muto, A., Ohkura, M., Abe, G., Nakai, J. and Kawakami, K. (2013). Real-Time Visualization of Neuronal Activity during Perception. *Current Biology* 23, 307–311.
- [Perlin, 1985] Perlin, K. (1985). An image synthesizer. In Proceedings of the 12th annual conference on Computer graphics and interactive techniques SIGGRAPH '85 pp. 287–296, Association for Computing Machinery, New York, NY, USA.
- [Rajan et al., 2016] Rajan, K., Harvey, C. and Tank, D. (2016). Recurrent Network Models of Sequence Generation and Memory. *Neuron* 90, 128–142.
- [Roxin et al., 2005] Roxin, A., Brunel, N. and Hansel, D. (2005). Role of Delays in Shaping Spatiotemporal Dynamics of Neuronal Activity in Large Networks. *Physical Review Letters* 94, 238103.
- [Shein-Idelson et al., 2017] Shein-Idelson, M., Pammer, L., Hemberger, M. and Laurent, G. (2017). Large-scale mapping of cortical synaptic projections with extracellular electrode arrays. *Nature Methods* 14, 882–890.
- [Spreizer et al., 2019] Spreizer, S., Aertsen, A. and Kumar, A. (2019). From space to time: Spatial inhomogeneities lead to the emergence of spatiotemporal sequences in spiking neuronal networks. *PLOS Computational Biology* 15, e1007432.
- [Sussillo and Abbott, 2009] Sussillo, D. and Abbott, L. F. (2009). Generating Coherent Patterns of Activity from Chaotic Neural Networks. *Neuron* 63, 544–557.
- [York and van Rossum, 2009] York, L. C. and van Rossum, M. C. W. (2009). Recurrent networks with short term synaptic depression. *Journal of Computational Neuroscience* 27, 607.